Contents lists available at ScienceDirect

Applied Catalysis B: Environment and Energy

Selective hydroprocessing of diphenyl ether into benzene over *in situ* generated MoOx and WOx

Mariyam Mukhtarova [*], Maria A. Golubeva [*], Alexey A. Sadovnikov, Anton L. Maximov

A.V. Topchiev Institute of Petrochemical Synthesis, Russian Academy of Sciences, Leninsky Prospekt, 29, Moscow 119991, Russia

ARTICLE INFO

ABSTRACT

The catalytic activity of molybdenum and tungsten oxides formed *in situ* from their carbonyls was studied in the hydroprocessing of diphenyl ether (DPE) for the first time. The MoOx and WOx catalysts obtained were characterized by XRD, XPS, HRTEM, EDX, Raman spectroscopy, and NH3—TPD. The effect of various parameters on the substrate conversion and the yields of products was investigated. Oxygen vacancies (OVs) on the catalyst surface were found to be active sites in the DPE hydroprocessing. MoOx was more active than WOx due to more OVs on the surface of the catalyst. Benzene was obtained as a major product over both of catalysts with a highest yield of 87% (99% DPE conversion) over MoOx and of 69% (96% DPE conversion) over WOx.

1. Introduction

Nowadays, the conversion of lignin into valuable chemicals such as aromatics is one of the main challenges of green chemistry [1–3]. Lignin is an aromatic biopolymer, which consists of phenylpropane units linked by various aryl—O—aryl bonds (α—O—4, β—O—4 and 4—O—5) [1]. Moreover, the dissociation energy of the 4—O—5 bond is the highest and, therefore, difficult to be cleaved [4,5]. As known, there are two typical reaction routes in the hydroprocessing of lignin derivatives: hydrogenolysis–hydrogenation and hydrodeoxygenation [2,6]. The first route leads to the formation of hydrogenated compounds, and the second one to aromatics [7]. The hydrodeoxygenation route is preferable and allows producing valuable aromatic chemicals from a renewable source, lignin [8].

Traditional catalysts for the conversion of lignin derivatives are noble metals and transition metal sulfides, which demonstrate high efficiency in hydroprocessing of various lignin model compounds. In general, noble metal catalysts exhibit high selectivity for hydrogenated products and low selectivity for aromatics [9–12]. Additionally, their high cost limits their application. Sulfide catalysts rapidly oxidize to corresponding oxides or sulfoxides and require the addition of sulfiding agents to maintain activity [13]. Thus, many challenges associated with the development of alternative efficient catalysts for the hydroprocessing of lignin and its derivatives remain. Such catalysts as transition metal phosphides, oxides, and carbides possess the following advantages: a low cost and high selectivity for deoxygenated aromatics

[14]. As known, anion vacancies in transition metal compounds favor hydrodeoxygenation route with the high yield of aromatics [2,15]. For instance, oxygen vacancies (OVs) can be produced by the reduction of metal oxides in H_2 atmosphere during hydroprocessing [16]. The existence of OVs can be estimated by the combination of the X-ray photoelectron spectroscopy (XPS) method and the Raman spectroscopy method. In a number of works, the content of OVs was estimated by the XPS, using the spectra in in Mo 3d, W 4 f (by content of M^{5+}, M = Mo or W), and O 1 s regions [17–22]. Moreover, the different activity of metal oxide catalysts in the hydrodeoxygenation reaction can be explained by the different content of OVs. The Raman spectroscopy can also be used to demonstrate the evolution of OVs and compare the performance of catalysts. Yang et al. compared the content of OVs on the surface of Pt/WOx and Pt/0.1Al-WOx catalysts based on the position of the bands in the Raman spectra. It was reported that the greater shift of the peak from 717 cm^{-1} to 709 cm^{-1} of Pt/0.1Al-WOx catalyst than that from 717 cm^{-1} to 714 cm^{-1} of Pt/WOx catalyst demonstrates that more OVs are formed in Pt/0.1Al-WOx than that in Pt/WOx [23].

Some results on the hydroprocessing of lignin-derived compounds over molybdenum and tungsten oxide catalysts are shown in Table 1. Molybdenum oxide catalysts were studied in the hydrodeoxygenation of phenol [7], anisole [7,24,25], cresol [7,26], etc. The catalytic activity in the hydrodeoxygenation of various lignin derivatives was closely associated with the presence of OVs. As can be seen from Table 1, tungsten oxide is commonly used as doped with noble metals, which significantly affects the catalytic activity of such catalysts [27,28]. However, pure

---

* Corresponding authors.
E-mail addresses: mukhtarova@ips.ac.ru (M. Mukhtarova), vinnikova@ips.ac.ru (M.A. Golubeva).

tungsten oxide can also be considered as a catalyst for the hydroprocessing of model lignin compounds [29]. It can be concluded that molybdenum and tungsten oxides catalysts have high catalytic activity (conversion above 70%) and high selectivity for deoxygenation products.

As shown, most of the works are devoted to the study of the hydroprocessing of monomeric lignin model compounds. However, the understanding of the aryl-O-aryl dimer transformations makes it possible to proceed to the direct hydroprocessing of lignin.

In this work, we investigated the hydroprocessing of diphenyl ether (DPE) using molybdenum and tungsten oxides formed in situ from corresponding carbonyls during the hydroprocessing of the substrate. Such approach eliminates the stage of catalyst synthesis, thereby simplifying the process. In our previous work [29], oxide catalysts synthesized using this approach were applied for guaiacol (a monomeric derivative of lignin) hydrodeoxygenation into aromatic hydrocarbons (benzene, toluene, and xylenes). In the present paper, DPE transformation regularities were found, and, as a result, benzene, being the target product, was obtained with high selectivity, particularly when MoO_x was used as a catalyst (Table 1). The catalytic activity of in situ WO_x in the DPE conversion into benzene was demonstrated for the first time. Recently, DPE conversion to benzene was investigated over ex situ MoO_3 [7,30]. Zhang et al. studied the activity of MoO_3 in the hydrodeoxygenation of different phenolic compounds. In the case of diphenyl ether, the conversion was 71.8% with 93.8% selectivity for benzene [7]. Prasomsri et al. reported that the conversion of DPE using MoO_3 was 82.6% with 72.8% selectivity for benzene [30]. Moreover, for the first time, the evolution of OVs on the surface of each catalyst and their key role as active sites in the hydrodeoxygenation of DPE was shown and described for MoO_x and WO_x. The different performance of both catalysts in the hydroprocessing of DPE under the same conditions was explained by the different content of OVs.

2. Experimental

2.1. Materials

Molybdenum hexacarbonyl (LLC «Redkino experimental plant», Redkino, Russia, 36.5–37.5 wt% of Mo) and tungsten hexacarbonyl (LLC «Redkino experimental plant», Redkino, Russia, 51–52% wt% of W) were used as precursors for catalysts preparation. Diphenyl ether (JCS «VEKTON», Saint Petersburg, Russia, pur.), benzylphenyl ether («Angene», London, England, 98%), (2-phenoxyethyl)benzene («abcr GmbH», Karlsruhe, Germany, 96%) were used as substrates, and dodecane (Sigma-Aldrich, Burlington, VT, USA, >99%) was used as a solvent. Acetone (Component-reaktiv, Moscow, Russia, >99.5%) and petroleum ether 40/70 (Component-reaktiv, Moscow, Russia, tech.) were used for catalyst washing. The used gases were H_2 (≥98%, Air Liquide, Paris, France) and Ar (≥98%, Air Liquide, Paris, France).

2.2. Catalytic Tests

Both catalysts were prepared *in situ* in a stainless-steel autoclave reactor during the hydroprocessing of substrates. The hydroprocessing of DPE was carried out at the various molar ratios of substrate/metal = 5, 10, 20. A mixture of 2 g DPE solution (10 wt% in dodecane) and metal carbonyl ($Mo(CO)_6$ or $W(CO)_6$) was loaded to the reactor. The reaction was studied at 300–380 °C, under the initial pressure of H_2 1–5 MPa, for 1–6 h while undergoing constant magnetic stirring (7000 rpm). The hydroprocessing of benzylphenyl ether (BPE) and (2-phenoxyethyl)benzene (PPE) was carried out at 380 °C, 5 MPa H_2, for 6 h, at molar ratio of substrate/metal = 5.

After the reaction, the autoclave was cooled to a room temperature. Liquid reaction products were separated from the catalysts by centrifugation (5000× g rpm). *In situ* obtained catalysts were washed with petroleum ether and acetone. Then, the catalysts were dried and kept in an Ar atmosphere at room temperature. The catalysts obtained were marked as MoO_x and WO_x.

Table 1
Results on the hydroprocessing of lignin derivatives over molybdenum oxide and tungsten oxide containing catalysts.

Catalyst	Substrate	Reaction conditions	Conversion (%)	Selectivity (%)	Ref.
MoO_3	Guaiacol	340 ℃, 0.5 MPa H_2+3 MPa N_2, 6 h, autoclave	98.0	72.8 for benzene	[7]
	Anisole		98.2	69.5 for benzene	
	o-Cresol		78.9	82.6 for toluene	
	Eugenol		96.4	71.5 for allylbenzene	
	Vanillin		97.6	45.3 for benzene	
	Diphenyl ether		71.8	93.8 for benzene	
MoO_x/Al_2O_3	m-Cresol	340 ℃, 4 MPa H_2, υ_{H2} = 2.7 mL/h, υ_{feed} = 5.55 mL/h, fixed-bed reactor	22.1	85.5 for toluene	[26]
$MoO_x/SBA-15$			23.9	82.8 for toluene	
MoO_x/SiO_2			23.8	81.9 for toluene	
MoO_3/ZrO_2	Anisole	340 ℃, 0.5 MPa H_2, H_2/anisole = 50, space time = 125–230 kg_{cat}·s/$mol_{anisole}$, fixed-bed reactor	40	34.4 for benzene	[24]
MoO_3	Anisole	320 ℃, space time = 0.035 g_{cat}·h/$mmol_{feed}$, vapour-phase packed-bed flow reactor	78.7	44 for benzene	[30]
	Guaiacol		74.2	31.1 for phenol	
	Diphenyl ether		82.6	71.8 for benzene	
	m-Cresol		48.9	48.6 for toluene	
MoO_3/TiO_2	Phenol	350 ℃, WHSV = 0.27 g_{phenol}/cm^3_{cat}, υ_{H2} = 100 mL/min, fixed-bed continuous flow reactor	30	90 for benzene	[31]
MoO_2	p-Cresol	325 ℃, 4.14 MPa H_2, 4.67 h, autoclave	30	60 for toluene	[13]
MoO_3			80	60 for toluene	
$5Ru-30WO_x/$ SiAl	Phenol	220 ℃, 1 MPa H_2, 1 h, Parr reactor	100	77 for benzene	[27]
	p-Cresol		100	83 for benzene	
$5Ru-30WO_x/$ SiAl	Guaiacol	250 ℃, 1.6 MPa H_2, 1.5 h, Parr reactor	100	79 for benzene	[27]
$Pt-WO_x/C$	m-Cresol	350 ℃, 0.1 MPa H_2, υ_{H2} = 12 mL/min, WHSV = 60 h^{-1}, fixed-bed continuous flow reactor	61	98 for toluene	[28]
MoO_x	Diphenyl ether	380 °C, 1 MPa H_2, 6 h, autoclave	99	88 for benzene	This work
WO_x		380 °C, 5 MPa H_2, 6 h, autoclave	96	72 for benzene	

2.3. Characterization

The catalysts obtained were characterized by powder X-ray diffraction (XRD), X-ray photoelectron spectroscopy (XPS), high-resolution transmission electron microscopy (HRTEM), energy-dispersive X-ray (EDX) spectroscopy, Raman spectroscopy, and NH_3 temperature-programmed desorption (NH_3—TPD). The XRD patterns were recorded using Rigaku Rotaflex RU-200 diffractometer (CuKα radiation). The PDF-2 ICDD database of powder diffraction patterns was used for the qualitative phase analysis of the samples. The average crystallite sizes were estimated using the Scherrer equation. X-ray photoelectron spectra were recorded on a PREVAC EA15 electronic spectrometer using AlK$_α$ radiation (h$ν$ = 1486.74 eV, 150 W). The spectra were deconvoluted using PeakFit program. HRTEM with EDX spectroscopy (a field emission electron gun operated at 200 kV) were carried out using FEI Tecnai Osiris. The Raman spectra were taken on a Senterra II spectrometer (laser power 0.25 mW, wavelength 532 nm, magnification 50x). The acidity of the *in situ* obtained catalysts was determined by NH_3—TPD using a UNISIT USGA-101 (Russia) gas chemisorption analyzer.

The investigation of gaseous carbon-containing products obtained after catalytic reactions was carried out using a Chromos GH-1000 chromatograph equipped with a thermal conductivity detector. Helium was used as a carrier gas. Liquid reaction products were identified by gas chromatography–mass spectrometry (Thermo Scientific ISQ 7000 GC-MS) equipped with a Restek 5XI-17SIL MS CAP capillary column (30 m × 0.25 mm × 0.25 μm), and were quantified using gas chromatograph (Crystallux 4000 M) equipped with a flame ionization detector and an Optima-1 capillary column (25 m × 0.32 mm × 0.35 μm). Helium used as a carrier gas. The NetChromWin program was used to obtain and analyze the chromatograms. The conversion of substrate (%) and yield of products (%) were calculated using the following equations:

$$\text{Conversion of substrate}(\%) = \frac{\text{mole of substrate consumed}}{\text{initial mole of substrate}} \times 100\%,$$

$$\text{Yield}(\%) = \frac{\text{mole of product}}{\text{initial mole of substrate}} \times 100\%.$$

3. Results and discussion

3.1. Catalyst characterization

3.1.1. XRD

MoO_x and WO_x were obtained *in situ* from corresponding carbonyls during the hydroprocessing of DPE. Fig. 1a,b shows the XRD patterns of MoO_x and WO_x catalysts obtained at 380 °C, under 5 MPa H_2, and for 1–6 h. MoO_x samples are amorphous at all reaction times, that was also observed in our previous work [29]. In the case of WO_x, there are characteristic peaks related to WO_2 (PDF № 71–614). The peaks observed at the 2θ of 26.2, 37.2, 53.4, 60.3, 66.5 can be ascribed to the (011), (020), (220), (031), (202) lattice planes of WO_2, respectively [32, 33]. A rise in reaction time from 1 to 6 h contributes to an increase in the average crystallite size: 11±1 nm after 1 h, 13±2 nm after 3 h, and 13 ±1 nm after 6 h. Thus, increasing the reaction time promotes a slight growth of WO_x crystallites.

To identify the moment of carbonyl complete transformation into oxides, the XRD was carried out for the catalysts obtained at 300 °C, under 5 MPa H_2, after 30 min – 3 h. Since MoO_x was amorphous, the additional investigations were carried out only for WO_x (Figure S1). According to the XRD results, there are no reflections of initial carbonyl or oxide after 30 min. The sample was shown to be amorphous. The characteristic peaks related to WO_2 phase (PDF № 71–614) were found for the samples obtained after 1 and 3 h. Wide reflections in the sample
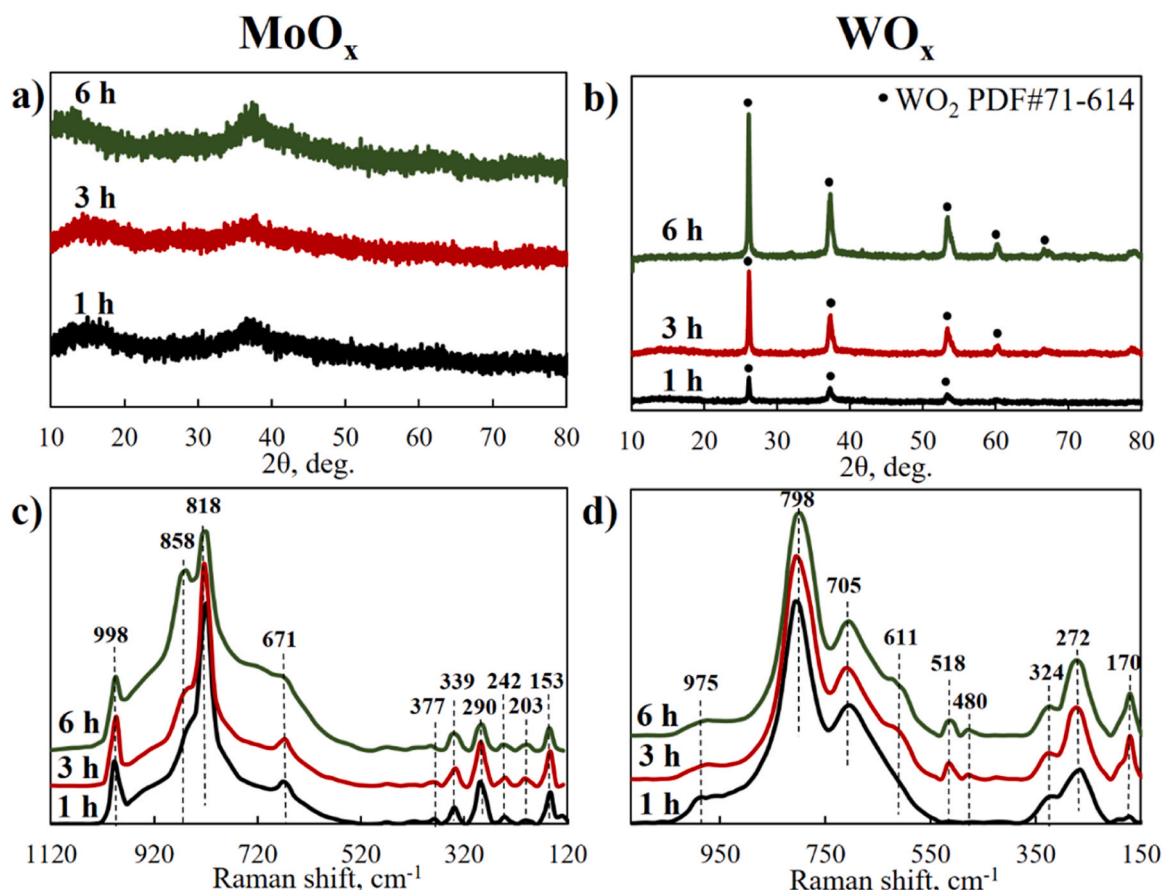

Fig. 1. The XRD patterns of a) MoO_x and b) WO_x. Raman spectra of c) MoO_x and d) WO_x. Reaction conditions: 10 wt% of DPE in dodecane, 380 °C, 5 MPa H_2, 1–6 h.

obtained after 1 h may be associated with small particle sizes of catalyst.

Since, only oxide phases were identified in the catalyst by the XRD and no carbon-containing phases (for example, carbides) were detected, additional analysis of gaseous carbon-containing products was carried out to confirm the formation of CO or other gases during the decomposition of metal carbonyls. The results are presented in Table S7 and confirmed other works in this area [34–38]. CH_4, CO and CO_2 (in trace amounts) were found as carbon-containing gases. The formation of CH_4 was due to the reduction of CO under H_2.

3.1.2. Raman spectroscopy

The catalysts obtained were also investigated by the Raman spectroscopy (Fig. 1c, d). The observed bands and their attributions are listed in Table S1 for MoO_x and Table S2 for WO_x. In the Raman spectra of MoO_x the bands at 998 and 818 cm^{-1} are attributed to the stretching modes of Mo=O [39,40] and O=Mo=O [39,41] in MoO_2, respectively. The intensity of these bands slowly increases with increasing of reaction time, which can be explained by producing MoO_2 with an increase in time. The sharp increase in band intensity at 858 cm^{-1} is observed after 6 h; this fact can be associated with the production of OVs during the reduction of MoO_3 to MoO_{3-x} [42]. There are two low-intensity bands at 339 and 203 cm^{-1}, which can be assigned to the bending modes of Mo–O [43] and O=Mo=O [44,45] in MoO_2. Vasilopoulou et al. reported, that the bands at 340−350 cm^{-1} can also be associated with generation of oxygen vacancies over molybdenum oxide and can be assigned to the stretching mode of Mo−Mo bond [46]. Moreover, the Raman bands at 671 [47,48], 377, 290, 242 and 153 cm^{-1} [49] are attributed to the different modes in MoO_3, the intensity of which decreases with increasing reaction time. The Raman spectrum of MoO_x is in good agreement with the spectrum of MoO_2 [39,50]. However, there are several bands corresponding to MoO_3. According to the results of Raman, in situ obtained MoO_x is crystalline, which contradicts the XRD results. This difference can be explained by the crystallization of amorphous molybdenum oxide under the action of laser power [47]. Fig. 1d represents the Raman spectra of WO_x obtained at different reaction time of 1−6 h (380 °C, 5 MPa H_2). There are characteristic bands of WO_2 at 798, 705, 611, 518, 480, 324, 272, 170 cm^{-1} at all conditions (Table S2) [32,51,52]. It should be noted that an increase in band intensity at 480 [53,54] and 324 cm^{-1} [51,55] are associated with producing OVs (W^{5+}=O) with an increase in the reaction time. Furthermore, there is a band of slight intensity at 975 cm^{-1}, that can be related to the low content of WO_3 and decreases with a rise in the reaction time by the reduction of W^{6+} to W^{5+}/W^{4+} [54]. Based on the above results of XRD and Raman, the intensity of all characteristic signals of WO_2 increases with enhancing reaction time from 1 to 6 h due to the decomposition of $W(CO)_6$ to WO_3 and further to WO_2.

3.1.3. XPS

The XP-spectra of MoO_x (Mo 3d) and WO_x (W 4 f) obtained at various reaction time are shown in Fig. 2. The all spectra of MoO_x in Mo 3d region include Mo in three oxidation states, such as Mo^{6+}, Mo^{5+} and Mo^{4+}. The peaks at 228.5—228.7 eV ($3d_{5/2}$) and 231.0—231.3 eV ($3d_{3/2}$) are attributed to Mo^{4+} in MoO_2 [39,56]. Another doublet at 229.6—230 eV ($3d_{5/2}$) and 233.2—233.6 ($3d_{3/2}$) is assigned to the Mo^{5+}
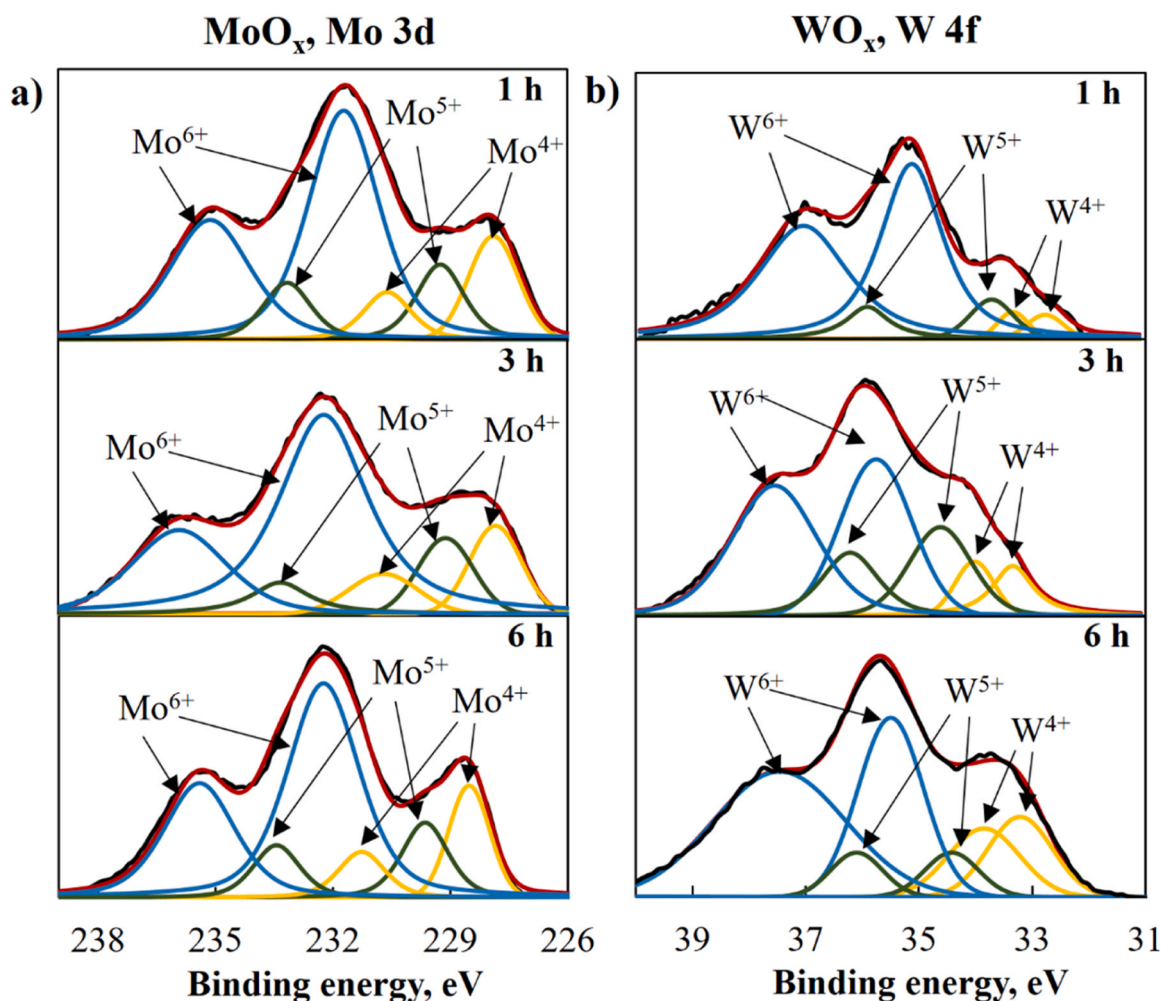

Fig. 2. The XPS of a) MoO_x in Mo 3d region, b) WO_x in W 4 f region. Reaction conditions: 10 wt% of DPE in dodecane, 380 °C, 5 MPa H_2, 1–6 h.

[57]. The presence of Mo^{5+} indicates the formation of OVs, which act as active sites in hydrodeoxygenation reactions [57]. The two peaks located at 232.2—232.3 ($3d_{5/2}$) and 235.4 eV ($3d_{3/2}$) are related to Mo^{6+} in MoO_3 [48,57]. According to the XPS data, the content of Mo^{6+}, Mo^{5+}, and Mo^{4+} changes insignificantly with increasing the reaction time from 1 to 6 h (380 °C, 5 MPa H_2) (Table S3). Three oxidation states (W^{6+}, W^{5+}, W^{4+}) are also observed in the XP-spectra of WO_x. The peaks located at 32.9—33.2 eV ($4 f_{7/2}$) and 33.6—33.9 eV ($4 f_{5/2}$) are assigned to W^{4+} in WO_2 [58,59], while the doublet related to W^{5+} is observed at 34.0—34.4 ($4 f_{7/2}$) and 36.1—36.4 eV ($4 f_{5/2}$) [32]. Two peaks at around 35.5—35.8 eV and 37.5—38.0 eV correspond to the W^{6+} (WO_3) in $4 f_{7/2}$ and $4 f_{5/2}$ regions [32,59,60]. The content of W^{4+} and W^{5+} sharply increases with enhancing reaction time, which implied the producing of OVs on the surface of catalyst (Table 2 and Table S4) during the reduction of the W^{6+} to W^{4+} and W^{5+} [60].

The O 1 s spectra for MoO_x and WO_x are shown in Fig. 3 and deconvoluted into three peaks for both catalysts. In the case of MoO_x, the peak centered at 529.9—530.2 eV belongs to Mo-O in MoO_3/MoO_2 [35, 61,62]. The peaks at 530.4—530.6 and 531.6—532 eV are assigned to the OVs [61,63,64] and to Mo—OH on the catalyst surface [34,64], respectively. A gradual increase in OVs content is observed due to the conversion of MoO_3 to MoO_2, which is also confirmed by Raman spectroscopy (Table 2 and Table S5) [64–67]. As shown in Fig. 4b, the XP-spectra of WO_x obtained at different reaction times have peaks assigned to W—O (530.3—530.7 eV), OVs in WO_x (530.5—531.4 eV) and W—OH (531.5—532.5 eV) [59,68,69]. The presence of M—OH (Mo—OH and W—OH) is associated with the adsorption of water, that is formed during the hydroprocessing of DPE. An intense rise in the OVs content on the WO_x surface is observed with increasing the reaction time from 1 to 3 h (Table 2 and Table S5). This fact is shown by the Raman spectra and caused by the reduction of W^{6+} to W^{5+}/W^{4+} in H_2 atmosphere.

WO_x catalysts obtained after 30 min and 1 h (300 °C, 5 MPa) were also studied by the XPS (Figure S1, Table S6). For catalysts obtained after 30 min and 1 h, peaks corresponding to the $W^{\delta+}$ in W 4 f region were not observed, which indicated complete decomposition of tungsten carbonyl. The doublets of three oxidation states (W^{6+}, W^{5+}, W^{4+}) were observed after 30 min and 1 h and are related to various tungsten oxides (Table S6). Thus, according to the XRD and XPS results, the full decomposition of tungsten carbonyl was obtained after 30 min of reaction (300 °C, 5 MPa H_2).

3.1.4. NH₃—TPD

The NH_3—TPD curves of MoO_x (Figure S2) show desorption peaks for all reaction times are observed at around 200 °C and related to weak acid sites. A rise in the reaction time leads to an increase in the amount of desorbed NH_3 and, consequently, to an increase in the amount of acid sites on the MoO_x surface (Table S8). For WO_x, the desorption peak shifts from 200 to 250 °C with increasing the reaction time from 1 to 6 h. However, the amount of desorbed NH_3 sharply decreases with increasing the reaction time, which implied that the number of acid sites on the WO_x surface relatively decreases. The presence of H_2 and H_2O are reported to lead to formation of Brønsted acid sites (M—OH) over oxide surface, that act as active sites in isomerization and dehydration

reactions [26]. According to the XPS data in O 1 s region for WO_x, a decrease of W—OH species content is observed with increasing the reaction time (Table S5). Thus, the number of acid sites is decreased due to reducing the content of W—OH.

3.1.5. HRTEM

The HRTEM images of MoO_x obtained at different reaction times are shown in Fig. 4. The samples of MoO_x obtained after 1 h and 6 h (380 °C, 5 MPa H_2) represent agglomerates of particles. According to the microphotographs, the samples obtained after 1 h and 6 h are amorphous, that is also confirmed by XRD. However, some crystalline areas are observed. MoO_x obtained after 1 h has a crystal lattice with the interplanar spacing of 0.281 nm, which corresponds to the (212) plane in Mo_4O_{11} [70]. As shown in Fig. 4b, the crystal lattices with the interplanar spacing of 0.240 and 0.170 nm are observed in the microphotographs of MoO_x obtained after 6 h. The first value corresponds to (200) plane [71,72] and the second to (220) plane in MoO_2 [73]. According to the HRTEM results, $Mo(CO)_6$ decomposes to the Mo_4O_{11}, which is further reduced to MoO_2. However, the presence of MoO_3 and MoO_2 was observed by Raman. It can be concluded that $Mo(CO)_6$ undergoes the following transformations during the hydroprocessing of DPE: $Mo(CO)_6 \rightarrow MoO_3 \rightarrow Mo_4O_{11} \rightarrow MoO_2$.

Fig. 5 shows the HRTEM images of WO_x obtained after 1 h and 6 h. WO_x obtained after 1 h represents agglomerates of particles and contains nanorods around them (Fig. 6a-d). Nanorods possess the crystal lattices with the interplanar spacing of 0.382 nm, which corresponds to the (010) plane in $W_{18}O_{49}$ [74]. Moreover, the value of the 0.239 nm interplanar spacing corresponds to (002) plane in WO_2 [68]. In the case of the sample obtained after 6 h, no nanorods are observed (Fig. 5e-f). However, the crystal lattice of WO_2 is seen (d = 0.239 nm (002) plane) (Fig. 5e). This fact indicates the full reduction of $W_{18}O_{49}$ to WO_2. Based on the results of XRD, Raman, and HRTEM, the following chain of W $(CO)_6$ transformations during hydroprocessing of DPE is observed: W $(CO)_6 \rightarrow WO_3 \rightarrow W_{18}O_{49} \rightarrow WO_2$. The elemental maps of MoO_x and WO_x obtained after various reaction times are shown in Figure S3 and Figure S5. The EDX spectra of both catalysts are shown in Figure S4 and Figure S6.

3.2. Catalytic activity

The hydroprocessing of DPE over *in situ* obtained MoO_x and WO_x were investigated under different conditions. The proposed routes of DPE hydroprocessing are shown in Fig. 6. Hydroprocessing of DPE begins with its hydrogenolysis into benzene and phenol over OVs [5,30, 75]. Then, phenol converts into benzene by its direct deoxygenation over OVs [25,30]. Further conversion of benzene is hydrogenation into cyclohexene. OVs were reported to act not only as active sites in hydrogenolysis/deoxygenation, but also in hydrogenation [13]. Cyclohexane and methylcyclopentane are the products of cyclohexene hydrogenation and can isomerize into each other over acid sites [76,77]. Moreover, cyclohexene can be formed by the dehydration of cyclohexanol over acid sites [26]. Cyclohexanol can be produced by phenol hydrogenation. The presense of Brønsted acid sites (M-OH) was confirmed by NH_3—TPD (Figure S1) and Lewis acid sites by XPS. The presence and evolution of OVs were confirmed by XPS and Raman. It was concluded, that the hydrodeoxygenation route was predominantly using *in situ* MoO_x and WO_x, benzene was the major product over both catalysts.

3.2.1. Effect of temperature

The influence of temperature was studied at 300—380 °C, under 5 MPa H_2, and for 6 h over both catalysts (Fig. 7a,b). In the case of MoO_x, the conversion of DPE was insignificantly changed with an increase in temperature and was 98—100%. The main reaction products was benzene; furthermore, cyclohexane and methylcyclopentane were formed. The yield of benzene gradually increased from 64% to 71% with
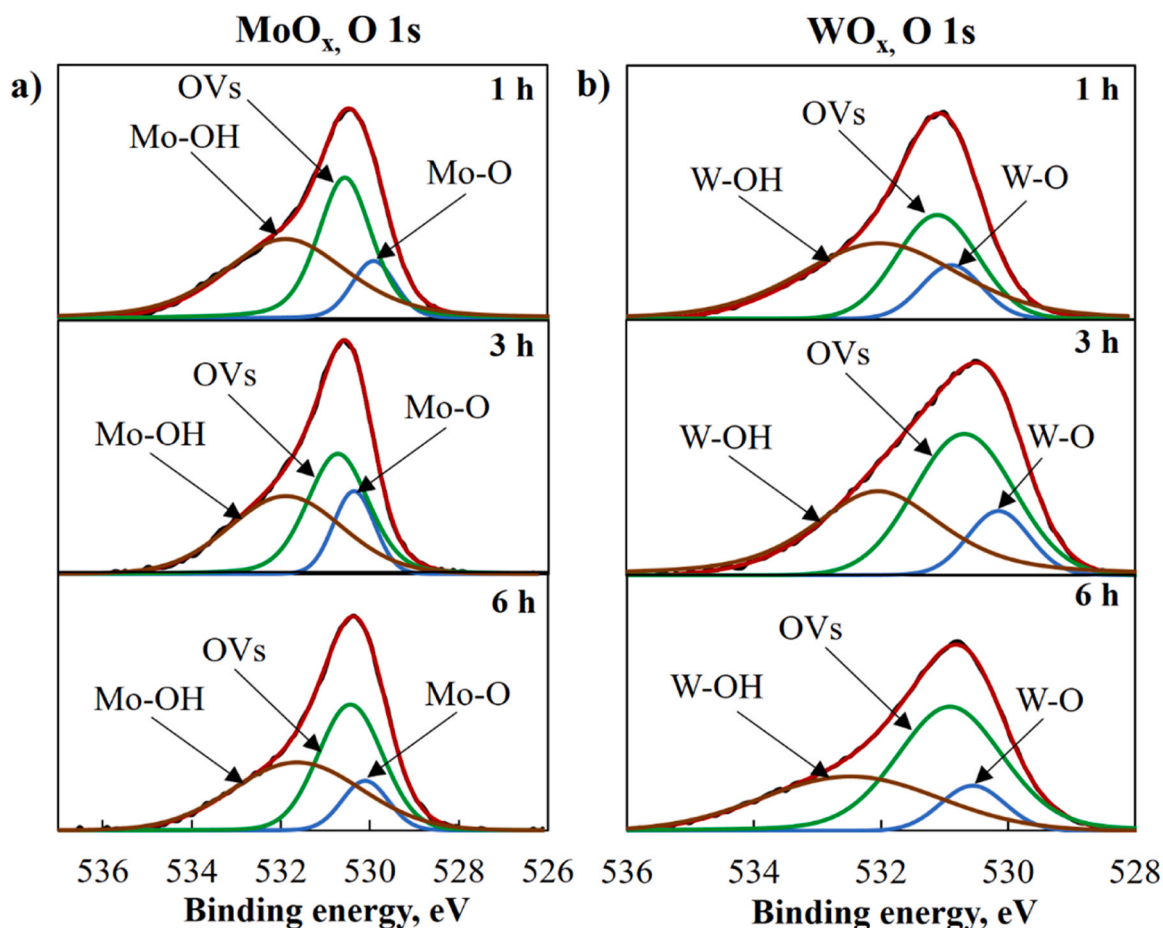
Table 2

XPS data of MoO_x and WO_x in O 1 s region. Reaction conditions: 10 wt% of DPE in dodecane, 380 °C, 5 MPa H_2, 1–6 h.

Time, h	MoO$_x$			WO$_x$		
	Mo—O	OVs	Mo—OH	W—O	OVs	W—OH
	Content (%)					
1	11	38	50	10	28	62
3	10	41	47	15	35	49
6	11	43	45	20	44	36

Fig. 3. XPS in O 1 s region of a) MoO_x b) WO_x. Reaction conditions: 10 wt% of DPE in dodecane, 380 °C, 5 MPa H_2, 1–6 h.

an increase in temperature from 300 to 380 °C, and the yield of phenol decreased from 10% to 1% due to its direct deoxygenation to benzene [24]. A decrease in the cyclohexane yield from 20% (300 °C) to 12% (380 °C) can be associated with its isomerization to methylcyclopentane [76,77], the yield of which increased from 2% (300 °C) to 15% (380 °C). Moreover, cyclohexane can also be formed during cyclohexene hydrogenation [24]. The conversion of DPE over WO_x catalyst rapidly increased from 15% (300°C) to 96% (380 °C). The products obtained were benzene, phenol and methylcyclopentane. An intense enhancing in the yields of benzene (from 6% to 69%) and methylcyclopentane (from 1% to 19%) was observed with a rise in temperature from 300 to 380 °C. The yield of phenol decreased from 7% to 1% due to its deoxygenation into benzene. Cyclohexane, cyclohexene and cyclohexanol are designated as other products. Cyclohexanol can be produced by phenol hydrogenation. Additionally, cyclohexanol could be an intermediate product that converts to cyclohexene . Alternatively, cyclohexene can be obtained by benzene hydrogenation [24]. Cyclohexene can be converted to cyclohexane and methylcyclopentane via hydrogenation. Compared to the MoO_x catalyst, WO_x showed a lower catalytic activity in DPE hydroprocessing under the same conditions. It can be explained by the less content of OVs over WO_x compared to MoO_x, that was observed in the XPS results.

3.2.2. Effect of reaction time

The effect of the reaction time on the product distribution and the DPE conversion was studied at 380 °C, under 5 MPa and for 1—6 h. Fig. 7c,d shows the yield of products and the conversion of DPE for various reaction time over MoO_x and WO_x. The conversion of DPE using MoO_x was quantitative over the entire time range. The yield of benzene decreased from 78% after 1 h to 65% after 6 h, that can be due to

benzene conversion to cyclohexene with subsequent hydrogenation to methylcyclopentane and cyclohexane (Fig. 7). Zhang et al. [24] reported that a decrease in benzene yield with increasing reaction time confirms that deoxygenation of phenol occurs before hydrogenation of the aromatic ring using MoO_x catalyst. In the case of WO_x, carrying out the reaction for 1 h made it possible to achieve only 47% conversion of DPE compared to full conversion over MoO_x at the same conditions. An increase in the reaction time from 3 to 6 h contributed to an increase in DPE conversion from 86% to 96%. The yield of benzene increased from 34% after 1 h to 69% after 6 h. The formation of benzene occurred during hydrogenolysis of DPE and the direct deoxygenation of phenol, the yield of which decreased from 7% (1 h) to 1% (6 h). The yield of methylcyclopentane increased from 4% to 19% as the reaction time increased from 1 to 6 h. Methylcyclopentane can be formed by isomerization of cyclohexane and hydrogenation/isomerization of cyclohexene.

Figure S9 shows the yield of products and the conversion of DPE for the reaction times of 15 and 30 min over MoO_x and WO_x. The conversion of DPE was 90% after 15 min and 99% after 30 min using MoO_x. Benzene was also the major product under both conditions; the yield of benzene was 71% and 76% after 15 min and 30 min, respectively. It is important to note that phenol was detected among the reaction products with low yields. In the case of WO_x, the conversion of DPE was significantly less (10% after 15 min and 42% after 30 min). The product distribution was the same as after 1—6 h.

Thus, the reaction time had a slight effect on the yield of products and the conversion of DPE using MoO_x. However, the catalytic activity of WO_x increased with a rise in the reaction time from 15 min to 6 h, which was caused by the formation of oxygen vacancies on the catalyst surface (confirmed by XPS and Raman).
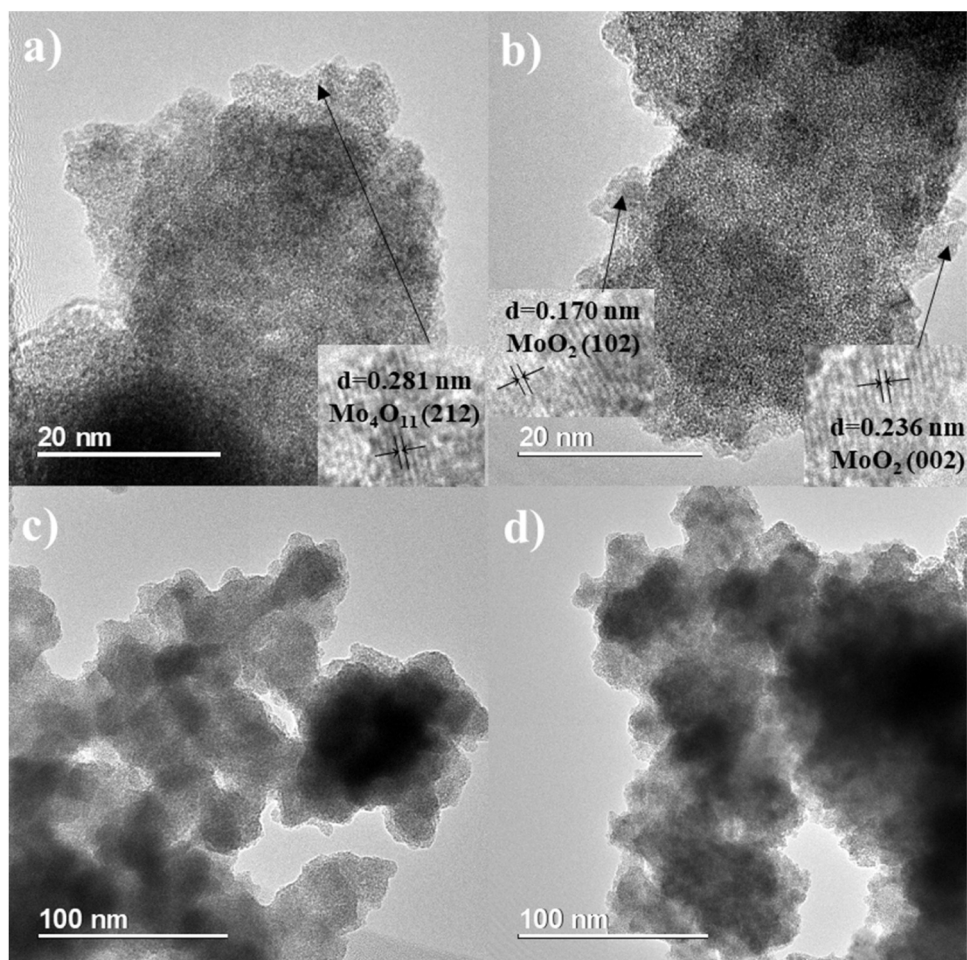
Fig. 4. The microphotographs of MoO$_x$ catalyst obtained a,c) after 1 h, b,d) after 6 h.
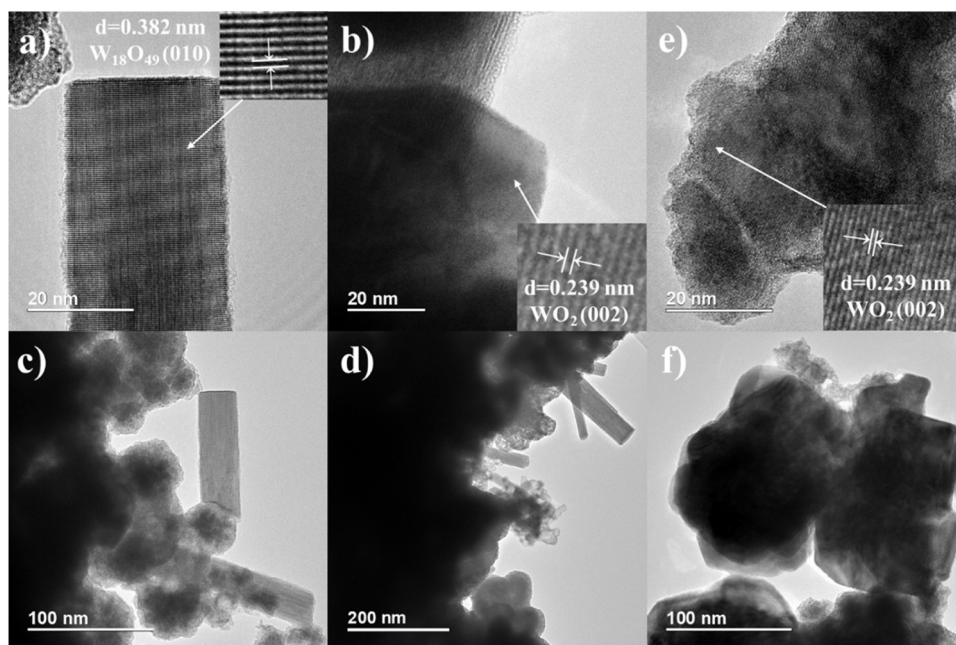

Fig. 5. The microphotographs of WO$_x$ catalyst obtained a—d) after 1 h, e—f) after 6 h.
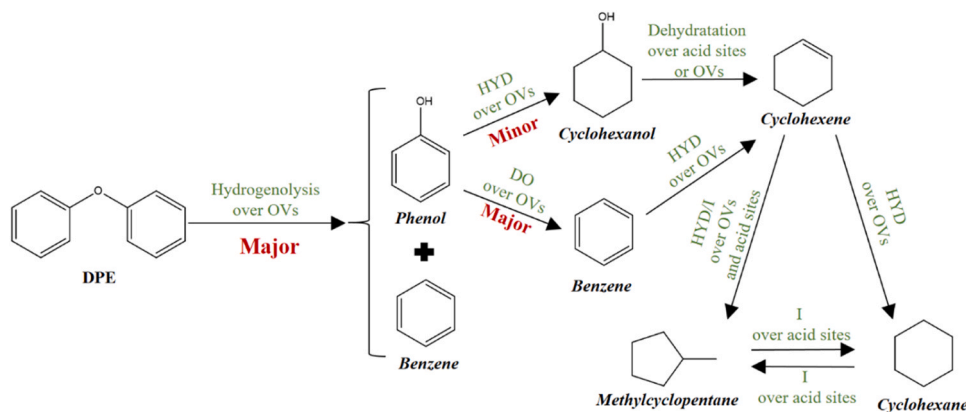
Fig. 6. Proposed scheme of DPE hydroprocessing over MoO_x and WO_x. HYD – hydrogenation, DO – deoxygenation, I – isomerization.
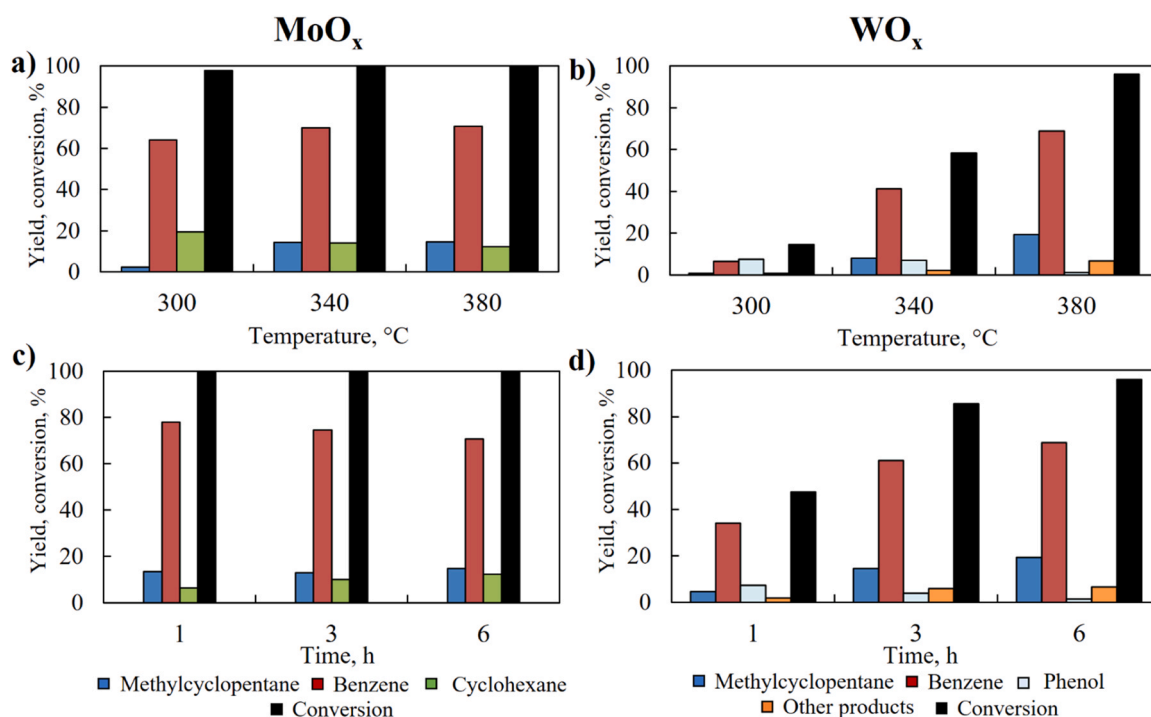

Fig. 7. Effect of temperature and reaction time on the product distribution and the conversion of DPE over a,c) MoO_x, b,d)WO_x. Reaction conditions: 10 wt% of DPE in dodecane, 300–380 °C, 5 MPa H_2, 1–6 h.

3.2.3. Effect of substrate/metal molar ratio

Influence of substrate/metal molar ratio on the hydroprocessing of DPE was investigated at 380 °C, 6 h, 5 MPa (Fig. 8a,b). The substrate/metal molar ratio was 5, 10 and 20. As shown in Fig. 8a, there is full conversion of DPE using MoO_x at all molar ratios. The yield of methylcyclopentane decreased from 15% to 6% as the molar ratio of substrate/metal increased from 5 to 20. However, the yield of benzene did not change and amounted to 70–71% at all molar ratios of substrate/metal. In the case of WO_x, the conversion of DPE rapidly decreased from 96 (a substrate/metal molar ratio = 5) to 56% (a substrate/metal molar ratio = 20), that was accompanied by a decrease in the yield of all products.

3.2.4. Effect of H_2 pressure

Fig. 8c,d shows the experimental results on the effect of H_2 pressure on DPE hydroprocessing under 1—5 MPa H_2 (380 °C, 6 h). These experiments were carried out at the substrate/metal ratio = 10 because of the highest cyclohexane yield at this ratio (20% over MoO_x). The conversion of DPE was 99—100% over MoO_x. The yield of benzene

decreased from 87% to 72% due to the formation of hydrogenated products such as cyclohexane and methylcyclopentane, the yield of which gradually increased. The conversion of DPE over WO_x under 1 MPa H_2 was only 10% and sharply increased to 93% under 5 MPa H_2. The generation of oxygen vacancies on the WO_x surface requires a higher H_2 pressure compared to MoO_x. Benzene was the main reaction product using WO_x. Methylcyclopentane and phenol were also found among the reaction products.

3.2.5. Comparative experiments

For comparison, experiments were carried out in the absence of a catalyst (380 °C, 5 MPa H_2, 6 h), as well as using a catalyst without H_2 pressure (Figure S10). The conversion of DPE without a catalyst was only 5%, while the benzene yield was 3%. MoO_x and WO_x demonstrated low catalytic activity in the absence of H_2. The conversion of DPE without H_2 was 11% and 3% over MoO_x and WO_x, respectively. However, according to XRD results, there are amorphous MoO_x and crystalline WO_2 in the absence of H_2, at 380 °C and for 6 h (Figure S7). To
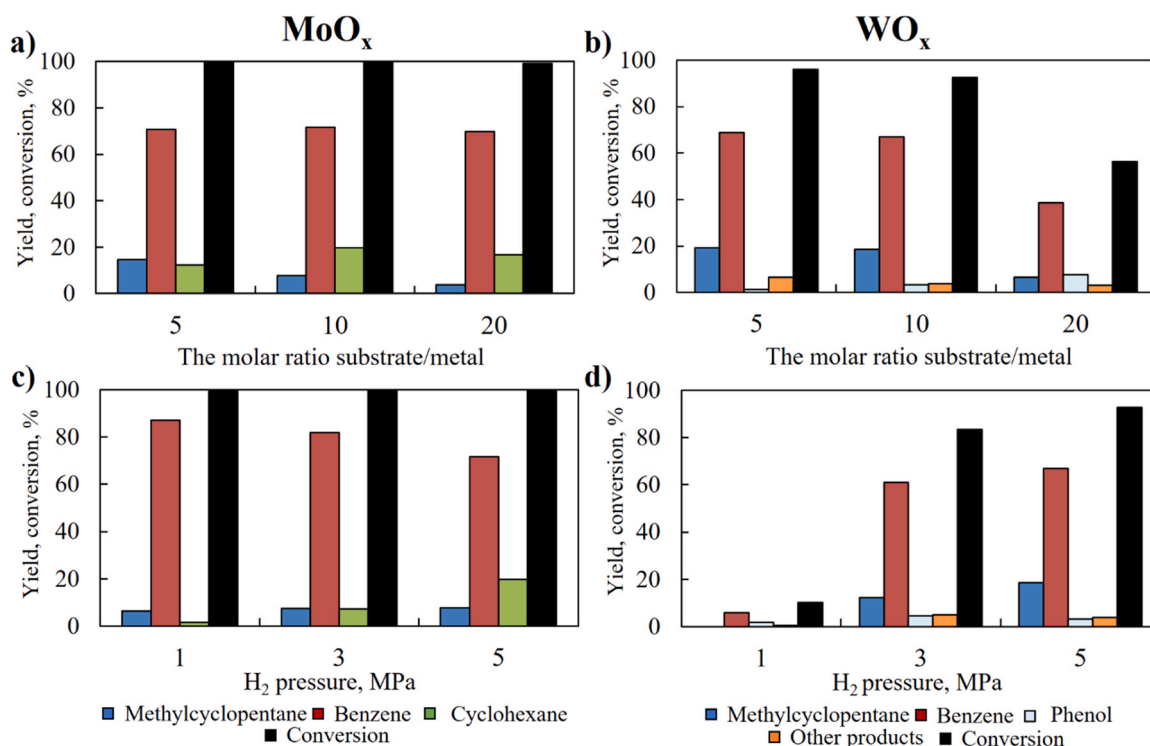
Fig. 8. Effect of molar ratio substrate/metal and hydrogen pressure on the product distribution and the conversion of DPE over a,c) MoO$_x$, b,d)WO$_x$. Reaction conditions: 10 wt% of DPE in dodecane, 380 °C, 1–5 MPa H$_2$, 1–6 h.

Table 3
The XPS data of MoO$_x$ and WO$_x$ in O 1 s region. Reaction conditions: 10 wt% of DPE in dodecane.

Catalyst	380 °C, 6 h	
	without H$_2$	5 MPa H$_2$
	Content of OVs (%)	
MoO$_x$	16	43
WO$_x$	14	44

explain the low catalytic activity in the absence of H$_2$, catalysts obtained were studied by XPS (Figure S8). According to the Table 3 and Table S9, catalysts contain significantly fewer oxygen vacancies compared to catalysts obtained at 5 MPa. This fact could be the reason for the low catalytic activity. In addition, DPE did not convert when the reaction was carried out without a catalyst and H$_2$ pressure (380 °C, 6 h, 0 MPa H$_2$). Thereby, the catalytic activity of molybdenum and tungsten oxide based catalysts is directly associated with the generation of oxygen

vacancies, which can be formed under H$_2$ pressure. Carrying out the reaction in the H$_2$ atmosphere also facilitates the hydrogenolysis and direct deoxygenation routes.

3.2.6. The recycling tests

The recycling tests of MoO$_x$ and WO$_x$ in DPE hydroprocessing were studied at medium values of the DPE conversion (Fig. 9). The experiments were carried out at 300 °C, 5 MPa H$_2$, 1 h over MoO$_x$ and at 380 °C, 5 MPa H$_2$, 1 h over WO$_x$. In the case of MoO$_x$, the conversion of DPE did not change after the first run, and slightly decreased from 49% after the second run to 38% after the fifth run. The yield of benzene also slowly decreased from 31% after the first run to 25% after the fifth run. The conversion of DPE over WO$_x$ catalyst insignificantly changed during the recycling tests. The yield of benzene was 28—34%. These results indicated that the *in situ* obtained molybdenum and tungsten oxides can be repeatedly used without significant loss in catalytic activity.

3.2.7. The hydroprocessing of BPE and PPE

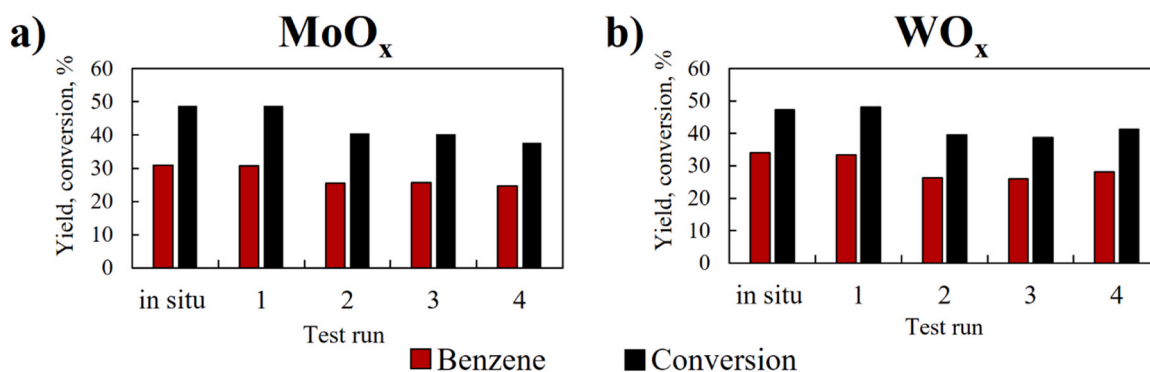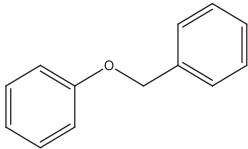Further, *in situ* obtained molybdenum and tungsten oxide based
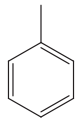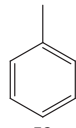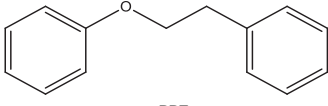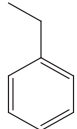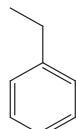

Fig. 9. The results of recycling tests of a) MoO$_x$ (300 °C, 5 MPa, 1 h), b) WO$_x$ (380 °C, 5 MPa, 1 h).

Table 4

The hydroprocessing of BPE and PPE over MoO_x and WO_x. Reaction conditions: 10 wt% of BPE or PPE in dodecane solution, 380 °C, 5 MPa H_2, 6 h.

Substrate	Conversion (%)		Yield of major products (%)	
	MoO_x	WO_x	MoO_x	WO_x
BPE	97	95	33 / 47	26 / 52
PPE	97	94	41 / 40	29 / 43

catalysts were tested in the hydroprocessing of BPE and PPE (380 °C, 5 MPa, for 6 h), that selected as model compounds for the 4—O—5 and β—O—4 bonds found in the structure of lignin [9,77]. The results of experiments are presented in Table 4. The hydroprocessing of BPE led to the formation of toluene and benzene. Whereas, ethylbenzene and benzene were formed during the hydroprocessing of PPE. Moreover, methylcyclopentane and cyclohexane were detected among the reaction products during the hydroprocessing of both substrates. Thus, *in situ* obtained molybdenum and tungsten oxides have shown excellent catalytic performance in the hydroprocessing of different model compounds of lignin. Hydrogenolysis and deoxygenation were the main pathways in the transformations of these substrates over MoO_x and WO_x catalysts.

4. Conclusions

The hydroprocessing of diphenyl ether was studied over MoO_x and WO_x formed *in situ* from their carbonyls in the reaction medium. The results of Raman spectroscopy, XPS, and HRTEM of MoO_x and WO_x indicated that the decomposition of $Mo(CO)_6$ occurred according to the following scheme: $Mo(CO)_6 \rightarrow MoO_3 \rightarrow Mo_4O_{11} \rightarrow MoO_2$, and the decomposition of $W(CO)_6$ along the following route: $W(CO)_6 \rightarrow WO_3 \rightarrow W_{18}O_{49} \rightarrow WO_2$. An increase in OVs content on the MoO_x and WO_x surfaces was observed with increasing the reaction time, as shown by the XPS and the Raman spectra.

Benzene was obtained from diphenyl ether with the highest yield of 87% at 99% conversion (380 °C, 1 MPa H_2, 6 h, S/Me=10) over MoO_x and 69% at 96% conversion over WO_x (380 °C, 5 MPa H_2, 6 h, S/Me=5). It was shown that the conversion of DPE without H_2 was very low (11% over MoO_x, and 3% over WO_x) due to the significantly lower content of OVs compared to the results obtained under 5 MPa H_2 (XPS data). In addition, the results of recycling tests indicated that the *in situ* obtained molybdenum and tungsten oxides can be repeatedly used without significant loss of activity. Moreover, *in situ* obtained MoO_x and WO_x

catalysts showed excellent catalytic performance in hydroprocessing not only DPE, but also other model dimer compounds of lignin (BPE, PPE).

Funding

CRediT authorship contribution statement

Anton L. Maximov: Writing – review & editing, Supervision, Conceptualization. **Alexey A. Sadovnikov:** Resources, Investigation. **Mariyam Mukhtarova:** Writing – review & editing, Writing – original draft, Visualization, Validation, Investigation, Formal analysis, Conceptualization. **Maria A. Golubeva:** Writing – review & editing, Validation, Supervision, Project administration, Conceptualization.

Declaration of Competing Interest

The authors declare that they have no known competing financial interests or personal relationships that could have appeared to influence the work reported in this paper.

Data availability

No data was used for the research described in the article.

Acknowledgements

Analytical center of deep oil processing and petrochemistry of the A.V. Topchiev Institute of Petrochemical Synthesis RAS and the JRC PMR IGIC RAS.

Appendix A. Supporting information

Supplementary data associated with this article can be found in the online version at doi:10.1016/j.apcatb.2024.123999.

References

[1] C. Cheng, D. Shen, S. Gu, K. Luo, State-of-the-art catalytic hydrogenolysis of lignin for the production of aromatic chemicals, Catal. Sci. Technol. 8 (2018) 6275–6296, https://doi.org/10.1039/C8CY00845K.

[2] J. Zhang, J. Sun, Y. Wang, Recent advances in selectively catalytic hydrodeoxygenation of lignin-derived oxygenates to arenes, Green Chem. 22 (2020) 1072–1098, https://doi.org/10.1039/C9GC02762A.

[3] M. Saidi, F. Samimi, D. Karimipourfard, T. Nimmanwudipong, B.C. Gates, M. R. Rahimpour, Upgrading of lignin-derived bio-oils by catalytic hydrodeoxygenation, Energy Environ. Sci. 7 (2014) 103–129, https://doi.org/10.1039/C3EE43081B.

[4] H. Zeng, D. Cao, Z. Qiu, C.-J. Li, Palladium-catalyzed formal cross-coupling of diaryl ethers with amines: slicing the 4-O -5 linkage in lignin models, Angew. Chem. Int. Ed. 57 (2018) 3752–3757, https://doi.org/10.1002/anie.201712211.

[5] X. Sun, Q. Xu, G. Kim, S.E. Flower, J.P. Lowe, J. Yoon, T.D. James, A water-soluble boronate-based fluorescent probe for the selective detection of peroxynitrite and imaging in living cells, Chem. Sci. 5 (2014) 3368, https://doi.org/10.1039/C4SC01417K.

[6] H.R. Rahimpour, M. Saidi, P. Rostami, B.C. Gates, M.R. Rahimpour, Experimental investigation on upgrading of lignin-derived bio-oils: kinetic analysis of anisole conversion on sulfided CoMo/Al₂O₃ catalyst, Int. J. Chem. Kinet. 48 (2016) 702–713, https://doi.org/10.1002/kin.21026.

[7] X. Zhang, J. Tang, Q. Zhang, Q. Liu, L. Li, L. Chen, L. Ma, Hydrodeoxygenation of lignin-derived phenolic compounds into aromatic hydrocarbons under low hydrogen pressure using molybdenum oxide as catalyst, Catal. Today 319 (2018) 41–47, https://doi.org/10.1016/j.cattod.2018.03.068.

[8] X. Huang, T.I. Korányi, M.D. Boot, E.J.M. Hensen, Ethanol as capping agent and formaldehyde scavenger for efficient depolymerization of lignin to aromatics, Green Chem. 17 (2015) 4941–4950, https://doi.org/10.1039/C5GC01120E.

[9] B. Güvenatam, O. Kurşun, E.H.J. Heeres, E.A. Pidko, E.J.M. Hensen, Hydrodeoxygenation of mono- and dimeric lignin model compounds on noble metal catalysts, Catal. Today 233 (2014) 83–91, https://doi.org/10.1016/j.cattod.2013.12.011.

[10] L. Zhang, Y. Wang, Y. Yang, B. Zhang, S. Wang, J. Lin, S. Wan, Y. Wang, Selective hydrogenolysis of aryl ether bond over Ru-Fe bimetallic catalyst, Catal. Today 365 (2020) 199–205, https://doi.org/10.1016/j.cattod.2020.04.030.

[11] B. Singh, R. Kumar, N. Singh, D. Tripathi, K. Natte, A. Narani, Hydrogenation of lignin-derived feedstocks and bio-oil using active and stable ruthenium catalyst, Catal. Today 408 (2023) 139–149, https://doi.org/10.1016/j.cattod.2022.07.013.

[12] W. Guan, X. Chen, C. Li, J. Zhang, C.-W. Tsang, H. Hu, S. Li, C. Liang, Nb(Ta)-based solid acid modified Pt/CNTs catalysts for hydrodeoxygenation of lignin-derived compounds, Mol. Catal. 467 (2019) 61–69, https://doi.org/10.1016/j.mcat.2019.01.015.

[13] V.M.L. Whiffen, K.J. Smith, Hydrodeoxygenation of 4-methylphenol over unsupported MoP, MoS₂, and MoOₓ catalysts, Energy Fuels 24 (2010) 4728–4737, https://doi.org/10.1021/ef901270h.

[14] Q. Bu, H. Lei, A.H. Zacher, L. Wang, S. Ren, J. Liang, R. Ruan, A review of catalytic hydrodeoxygenation of lignin-derived phenols from biomass pyrolysis, Bioresour. Technol. 124 (2012) 470–477, https://doi.org/10.1016/j.biortech.2012.08.089.

[15] M.M. Levitsky, A.I. Yalymov, A.N. Kulakova, A.A. Petrov, A.N. Bilyachenko, Cage-like metallasilsesquioxanes in catalysis: a review, J. Mol. Catal. A: Chem. 426 (2017) 297–304, https://doi.org/10.1016/j.molcata.2016.06.016.

[16] G. Huang, Y. Chen, Z. Zhuang, Y. Yu, J. Yu, Oxygen vacancies in metal oxides: recent progress towards advanced catalyst design, Sci. China Mater. 63 (2020) 2089–2118, https://doi.org/10.1007/s40843-020-1305-6.

[17] R. Kashfi-Sadabad, S. Yazdani, T.D. Huan, Z. Cai, M.T. Pettes, Role of oxygen vacancy defects in the electrocatalytic activity of substoichiometric molybdenum oxide, J. Phys. Chem. C 122 (2018) 18212–18222, https://doi.org/10.1021/acs.jpcc.8b03536.

[18] D.G. Dionizio, L. Forrer, G. Berhault, P.M. de Souza, C.A. Henriques, Enhancement of hydrodeoxygenation catalytic performance through the addition of copper to molybdenum oxide-based catalysts, Mol. Catal. 536 (2023) 112882, https://doi.org/10.1016/j.mcat.2022.112882.

[19] C. Yu, S. Yu, L. Li, Upgraded methyl oleate to diesel-like hydrocarbons through selective hydrodeoxygenation over Mo-based catalyst, Fuel 308 (2022) 122038, https://doi.org/10.1016/j.fuel.2021.122038.

[20] T. Hu, S.M. Gericke, X. Tong, D. Nykypanchuk, T. Kristensen, C. Hulteberg, D. Stacchiola, S. Blomberg, A.R. Head, Interaction of Anisole on Alumina-Supported Ni and Mo Oxide Hydrodeoxygenation Catalysts, J. Phys. Chem. C 127 (2023) 19440–19450, https://doi.org/10.1021/acs.jpcc.3c02780.

[21] R. Ding, Y. Wu, Y. Chen, H. Chen, J. Wang, Y. Shi, M. Yang, Catalytic hydrodeoxygenation of palmitic acid over a bifunctional Co-doped MoO₂/CNTs

[22] Z. Li, X. Lu, W. Sun, L. Leng, M. Zhang, H. Li, L. Bai, D. Yuan, J.H. Horton, J. Wang, One-step synthesis of single palladium atoms in WO₂.₇₂ with high efficiency in chemoselective hydrodeoxygenation of vanillin, Appl. Catal. B. 298 (2021) 120535, https://doi.org/10.1016/j.apcatb.2021.120535.

[23] M. Yang, K. Wu, S. Sun, Y. Ren, Regulating oxygen defects via atomically dispersed alumina on Pt/WOₓ catalyst for enhanced hydrogenolysis of glycerol to 1,3-propanediol, Appl. Catal. B. 307 (2022) 121207, https://doi.org/10.1016/j.apcatb.2022.121207.

[24] J. Dai, X. Xiao, S. Duan, J. Liu, J. He, J. Lei, L. Wang, Synthesis of novel microporous nanocomposites of ZIF-8 on multiwalled carbon nanotubes for adsorptive removing benzoic acid from water, Chem. Eng. J. 331 (2018) 64–74, https://doi.org/10.1016/j.cej.2017.10.090.

[25] T. Prasomsri, T. Nimmanwudipong, Y. Román-Leshkov, Effective hydrodeoxygenation of biomass-derived oxygenates into unsaturated hydrocarbons by MoO₃ using low H₂ pressures, Energy Environ. Sci. 6 (2013) 1732–1738, https://doi.org/10.1039/C3EE24360E.

[26] V.O.O. Gonçalves, C. Ciotonea, S. Arrii-Clacens, N. Guignard, C. Roudaut, J. Rousseau, F. Richard, Effect of the support on the hydrodeoxygenation of m -cresol over molybdenum oxide based catalysts, Appl. Catal. B 214 (2017) 57–66, https://doi.org/10.1016/j.apcatb.2017.05.003.

[27] Y.-B. Huang, L. Yan, M.-Y. Chen, Q.-X. Guo, Y. Fu, Selective hydrogenolysis of phenols and phenyl ethers to arenes through direct C–O cleavage over ruthenium–tungsten bifunctional catalysts, Green Chem. 17 (2015) 3010–3017, https://doi.org/10.1039/C5GC00326A.

[28] C. Wang, A.V. Mironenko, A. Raizada, T. Chen, X. Mao, A. Padmanabhan, J. M. Vohs, Mechanistic Study of the Direct Hydrodeoxygenation of m-Cresol over WOₓ-Decorated Pt/C Catalysts, ACS Catal. 8 (2018) 7749–7759, https://doi.org/10.1021/acscatal.8b01746.

[29] M. Mukhtarova, M. Golubeva, A. Sadovnikov, A. Maximov, Guaiacol to aromatics: efficient transformation over in situ-generated molybdenum and tungsten oxides, Catalysts 13 (2023) 263, https://doi.org/10.3390/catal13020263.

[30] T. Prasomsri, M. Shetty, K. Murugappan, Y. Román-Leshkov, Insights into the catalytic activity and surface modification of MoO₃ during the hydrodeoxygenation of lignin-derived model compounds into aromatic hydrocarbons under low hydrogen pressures, Energy Environ. Sci. 7 (2014) 2660–2669, https://doi.org/10.1039/C4EE00890A.

[31] S. Boullosa-Eiras, R. Lødeng, H. Bergem, M. Stöcker, L. Hannevold, E.A. Blekkan, Catalytic hydrodeoxygenation (HDO) of phenol over supported molybdenum carbide, nitride, phosphide and oxide catalysts, Catal. Today 223 (2014) 44–53, https://doi.org/10.1016/j.cattod.2013.09.044.

[32] C. Shu, S. Kang, Y. Jin, X. Yue, P.K. Shen, Bifunctional porous non-precious metal WO₂ hexahedral networks as an electrocatalyst for full water splitting, J. Mater. Chem. A 5 (2017) 9655–9660, https://doi.org/10.1039/C7TA01527E.

[33] C. He, H. Bai, W. Yi, J. Liu, X. Li, X. Li, G. Xi, A highly sensitive and stable SERS substrate using hybrid tungsten dioxide/carbon ultrathin nanowire beams, J. Mater. Chem. C 6 (2018) 3200–3205, https://doi.org/10.1039/C8TC00573G.

[34] H.S.O. Chan, T.S.A. Hor, C.S.M. Chiam, T.C. Chong, Thermal degradation of the transition metal carbonyl complexes: I. TG and DSC of monodentate bis-(diphenylphosphino)-methane substituted carbonyl complexes of chromium, molybdenum and tungsten, J. Therm. Anal. Calorim. 32 (1987) 1115–1126, https://doi.org/10.1007/BF01905166.

[35] D. Mahajan, E.T. Papish, K. Pandya, Sonolysis induced decomposition of metal carbonyls: kinetics and product characterization, Ultrason. Sonochem. 11 (2004) 385–392, https://doi.org/10.1016/j.ultsonch.2003.10.009.

[36] C.C. Cho, S.L. Bernasek, Molybdenum deposition from the decomposition of molybdenum hexacarbonyl, J. Appl. Phys. 65 (1989) 3035, https://doi.org/10.1063/1.342695.

[37] I. Usoltsev, R. Eichler, Y. Wang, J. Even, A. Yakushev, H. Haba, M. Asai, H. Brand, A. Di Nitto, C.E. Düllmann, F. Fangli, Decomposition studies of group 6 hexacarbonyl complexes. Part 1: production and decomposition of Mo(CO)₆ and W (CO)₆, Radiochim. Acta 104 (2016) 141–151, https://doi.org/10.1515/ract-2015-2445.

[38] L.H. Kaplan, F.M. d'Heurle, The deposition of molybdenum and tungsten films from vapor decomposition of carbonyls, J. Electrochem. Soc. 117 (1970) 693, https://doi.org/10.1149/1.2407607.

[39] Y. Qiu, S. Liu, C. Wei, J. Fan, H. Yao, L. Dai, X. Guo, Synergistic effect between platinum single atoms and oxygen vacancy in MoO₂ boosting pH-Universal hydrogen evolution reaction at large current density, Chem. Eng. J. 427 (2022) 131309, https://doi.org/10.1016/j.cej.2021.131309.

[40] R. Thangappan, M. Arivanandhan, S. Kalaiselvam, R. Jayavel, Y. Hayakawa, Molybdenum oxide/graphene nanocomposite electrodes with enhanced capacitive performance for supercapacitor applications, J. Inorg. Organomet. Polym. Mater. 28 (2017) 50–62, https://doi.org/10.1007/s10904-017-0699-1.

[41] S. Xie, D. Chen, C. Gu, T. Jiang, S. Zeng, Y. Wang, Z. Ni, X. Shen, J. Zhou, Molybdenum oxide/tungsten oxide nano-heterojunction with improved surface-enhanced raman scattering performance, ACS Appl. Mater. Interfaces 13 (2021) 33345–33353, https://doi.org/10.1021/acsami.1c03848.

[42] M.A. Camacho-López, L. Escobar-Alarcón, M. Picquart, R. Arroyo, G. Córdoba, E. Haro-Poniatowski, Micro-Raman study of the m-MoO₂ to α-MoO₃ transformation induced by cw-laser irradiation, Opt. Mater. 33 (2011) 480–484, https://doi.org/10.1016/j.optmat.2010.10.028.

[43] M.A. Py, P.E. Schmid, J.T. Vallin, Raman scattering and structural properties of MoO₃, Nuovo Cim. B 38 (1977) 271–279, https://doi.org/10.1007/bf02723496.

[44] J. He, C. Zhao, J.A. Lercher, Ni-Catalyzed Cleavage of Aryl Ethers in the Aqueous Phase, J. Am. Chem. Soc. 134 (2012) 20768–20775, https://doi.org/10.1021/ja309915e.

[45] G. Mestl, M. Dieterle, Raman spectroscopy of molybdenum oxides, Phys. Chem. Chem. Phys. 4 (2002) 822–826, https://doi.org/10.1039/B107046K.

[46] M. Vasilopoulou, A.M. Douvas, D.G. Georgiadou, L.C. Palilis, S. Kennou, L. Sygellou, A. Soultati, I. Kostis, G. Papadimitropoulos, D. Davazoglou, P. Argitis, The Influence of hydrogenation and oxygen vacancies on molybdenum oxides work function and gap states for application in organic optoelectronics, J. Am. Chem. Soc. 134 (2012) 16178–16187, https://doi.org/10.1021/ja3026906.

[47] K. Ajito, L.A. Nagahara, D.A. Tryk, K. Hashimoto, A. Fujishima, Study of the photochromic properties of amorphous MoO₃ films using Raman microscopy, J. Phys. Chem. 99 (1995) 16383–16388, https://doi.org/10.1021/j100044a028.

[48] I. De Castro Silva, A.C. Reinaldo, F.A. Sigoli, I.O. Mazali, Raman spectroscopy-in situ characterization of reversibly intercalated oxygen vacancies in α-MoO₃, RSC Adv 10 (2020) 18512–18518, https://doi.org/10.1039/d0ra01207f.

[49] P.A. Spevack, N.S. McIntyre, Thermal reduction of molybdenum trioxide, J. Phys. Chem. 96 (1992) 9029–9035, https://doi.org/10.1021/j100201a062.

[50] K. Kumari, Y.-R. Ma, C.-C. Tsai, Y.-W. Lin, S.Y. Wu, K.-W. Cheng, Y. Liou, X-ray diffraction and Raman scattering studies on large-area array and nanobranched structure of 1D MoO₂ nanorods, Nanotechnology 18 (2007) 115717, https://doi.org/10.1088/0957-4484/18/11/115717.

[51] I. Székely, M. Baia, K. Magyari, B. Boga, Z. Pap, The effect of the pH adjustment upon the WO₃-WO₃·0.33H₂O-TiO₂ ternary composite systems' photocatalytic activity, Appl. Surf. Sci. 490 (2019) 469–480, https://doi.org/10.1016/j.apsusc.2019.06.036.

[52] Y.-R Ma, C.-M. Lin, C.-L. Yeh, R.-T. Huang, Synthesis and characterization of one-dimensional WO₂ nanorods, J. Vac. Sci. Technol. B. 23 (2005) 2141–2145, https://doi.org/10.1116/1.2050668.

[53] N.E. Stankova, P.A. Atanasov, T.J. Stanimirova, A.O. Dikovska, R.W. Eason, Thin (001) tungsten trioxide films grown by laser deposition, Appl. Surf. Sci. 247 (2005) 401–405, https://doi.org/10.1016/j.apsusc.2005.01.057.

[54] H.-C. Chen, D.-J. Jan, Y.-S. Luo, K.-T. Huang, Electrochromic and optical properties of tungsten oxide films deposited with DC sputtering by introducing hydrogen, Appl. Opt. 53 (2014) 321, https://doi.org/10.1364/AO.53.00A321.

[55] I. Székely, E.-Z Kedves, Z. Pap, M. Baia, Synthesis Design of Electronegativity Dependent WO₃ and WO₃•0.33H₂O Materials for a Better Understanding of TiO₂/WO₃ Composites' Photocatalytic Activity, Catalysts.11 (2021) 779, https://doi.org/10.3390/catal11070779.

[56] J. Baltrusaitis, B. Mendoza-Sanchez, V. Fernandez, R. Veenstra, N. Dukstiene, A. Roberts, N. Fairley, Generalized molybdenum oxide surface chemical state XPS determination via informed amorphous sample model, Appl. Surf. Sci. 326 (2015) 151–161, https://doi.org/10.1016/j.apsusc.2014.11.0777.

[57] X. Zhou, H.-Y. Zhou, T.-Y. Cheang, Z.-W. Zhao, C.-C. Shen, K. Liang, A.-W. Xu, Monodisperse Pd Nanotetrahedrons on Ultrathin MoO₃₋ₓ Nanosheets as Excellent Heterogeneous Catalyst for Chemoselective Hydrogenation Reactions, J. Phys. Chem. C. 121 (2017) 27528–27534, https://doi.org/10.1021/acs.jpcc.7b10279.

[58] R. Wu, J. Zhang, Y. Shi, D. Liu, B. Zhang, Metallic WO₂–Carbon Mesoporous Nanowires as Highly Efficient Electrocatalysts for Hydrogen Evolution Reaction, Am. Chem. Soc. 137 (2015) 6983–6986, https://doi.org/10.1021/jacs.5b01330.

[59] K. Qian, L. Du, X. Zhu, S. Liang, S. Chen, H. Kobayashi, R. Li, Directional Oxygen Activation by Oxygen-Vacancy-Rich WO₂ Nanorods for Superb Hydrogen Evolution via Formaldehyde Reforming, J. Mater. Chem. A. 7 (2019) 14592–14601, https://doi.org/10.1039/C9TA03051D.

[60] F. Liu, X. Chen, Q. Xia, L. Tian, X. Chen, Ultrathin tungsten oxide nanowires: oleylamine assisted nonhydrolytic growth, oxygen vacancies and good photocatalytic properties, RSC Adv 5 (2015) 77423–77428, https://doi.org/10.1039/C5RA12993A.

[61] H. Li, H. Ye, Z. Xu, C. Wang, J. Yin, H. Zhu, Freestanding MoO₂/Mo₂C imbedded carbon fibers for Li-ion batteries, Phys. Chem. Chem. Phys. 19 (2017) 2908–2914, https://doi.org/10.1039/C6CP07569J.

[62] M. Sajadi, M. Ranjbar, R. Rasuli, Two-step synthesis of Ag-decorated MoO₃ nanotubes, and the effect of hydrogen doping, Appl. Surf. Sci.527 (2020) 146675, https://doi.org/10.1016/j.apsusc.2020.146675.

[63] B. Wang, Z. Zhang, S. Zhang, Y. Cao, Y. Su, S. Liu, M. Ma, Surface Excited MoO₂ to Master full Water Splitting, Electrochim. Acta. 359 (2020) 136929, https://doi.org/10.1016/j.electacta.2020.136929.

[64] Y. Cao, P. Liang, Q. Dong, D. Wang, D. Zhang, L. Tang, Z. Yu, A facile reduction method synthesis of defective MoO₂₋ₓ nanospheres used for SERS detection with highly chemical enhancement, Anal. Chem. 91 (2019) 8683–8690, https://doi.org/10.1021/acs.analchem.9b02394.

[65] X. Liu, L. Yang, M. Huang, Q. Li, L. Zhao, Y. Sang, X. Zhang, Z. Zhao, H. Liu, W. Zhou, Oxygen vacancy-regulated metallic semiconductor MoO₂ nanobelt photoelectron and hot electron self-coupling for photocatalytic CO₂ reduction in pure water, Appl. Catal., B. 319 (2022) 121887, https://doi.org/10.1016/j.apcatb.2022.121887.

[66] J.-Q. Wu, J.-W. Zhao, G.-R. Li, Highly Dispersed MoO₂ Nanoparticles Confined in N-doped Porous Carbon Nanosheets for Efficient Hydrogen Evolution in Alkaline Media, Energy Fuels 34 (2020) 9050–9057, https://doi.org/10.1021/acs.energyfuels.0c01358.

[67] P. Guha, B. Mohanty, R. Thapa, R.M. Kadam, P.V. Satyam, B.K. Jena, Defects Engineered MoO₂ Nanostructures as an Efficient Electrocatalyst for Oxygen Evolution Reaction, ACS Appl. Energy Mater. 6 (2020) 5208–5218, https://doi.org/10.1021/acsaem.9b02551.

[68] X. He, S. Bai, J. Jiang, W.-J. Ong, J. Peng, Z. Xiong, N. Li, Oxygen vacancy mediated step-scheme heterojunction of WO₂.₉/g-C₃N₄ for efficient electrochemical sensing of 4-nitrophenol, Chem. Eng. J. Adv. 8 (2021) 100175, https://doi.org/10.1016/j.ceja.2021.100175.

[69] S. Rahimnejad, J. Hui He, F. Pan, X. Lee, W. Chen, K. Wu, G. Qin Xu, Enhancement of the photocatalytic efficiency of WO₃ nanoparticles via hydrogen plasma treatment, Materials Research Express 1 (2014) 045044, https://doi.org/10.1088/2053-1591/1/4/045044.

[70] Y. Li, Z. Song, Y. Li, S. Li, H. Wang, B. Song, X. Du, Synthesis of Mo₄O₁₁@MoO₃ nanobelts and their improved sensing performance to NO₂ gas. Materials Research Express 6 (2019) 055041 https://doi.org/10.1088/2053-1591/ab0689.

[71] A. Khademi, R. Azimirad, A.A. Zavarian, A.Z. Moshfegh, Growth and Field Emission Study of Molybdenum Oxide Nanostars, The Journal of Physical Chemistry C 113 (2009) 19298–19304, https://doi.org/10.1021/jp9056237.

[72] B. Xu, Y. Li, G. Wang, D. Zhao, K. Pan, B. Jiang, H. Fu, In situ synthesis and high adsorption performance of MoO₂/Mo₄O₁₁ and MoO₂/MoS₂ composite nanorods by reduction of MoO₃, Dalton Trans 44 (2015) 6224–6228, https://doi.org/10.1039/c4dt03067b.

[73] M. Sarno, A. Garamella, C. Cirillo, P. Ciambelli, MoO₂ Synthesis for LIBs, Chem. Eng. Trans. 41 (2014) 307, https://doi.org/10.3303/CET1441052.

[74] C.L. Chen, H. Mori, In situ TEM observation of the growth and decomposition of monoclinic W₁₈O₄₉ nanowires, Nanotechnology 20 (2009) 285604, https://doi.org/10.1088/0957-4484/20/28/285604.

[75] X. Wang, R. Rinaldi, Bifunctional Ni catalysts for the one-pot conversion of Organosolv lignin into cycloalkanes, Catal. Today. 269 (2016) 48–55, https://doi.org/10.1016/j.cattod.2015.11.047.

[76] V.N. Bui, D. Laurenti, P. Afanasiev, C. Geantet, Hydrodeoxygenation of guaiacol with CoMo catalysts. Part I: Promoting effect of cobalt on HDO selectivity and activity, Appl. Catal. B. 101 (2016) 239–245, https://doi.org/10.1016/j.apcatb.2010.10.025.

[77] J. He, C. Zhao, J.A. Lercher, Ni-Catalyzed Cleavage of Aryl Ethers in the Aqueous Phase, J. Am. Chem. Soc. 134 (2012) 20768–20775, https://doi.org/10.1021/ja309915e.